RESEARCH | Article in Press

Modeling and simulation of human lung mechanics using single to multi-compartment electrical circuit models

Jimmy Nabende Wanzala · **Michael Robson Atim**

Received: 1 May 2026 / Accepted: 14 September 2026
© The Author(s) 2026

Abstract

This study focuses on the development, simulation, and comparative analysis of electrical analog models for representing human respiratory mechanics. The respiratory system was modeled using lumped parameter electrical circuits, where physiological variables such as pressure, airflow, lung compliance, airway resistance, and airway inertance were represented by voltage, current, capacitance, resistance, and inductance, respectively. Four distinct models: single-compartment, two-compartment, three-compartment, and multi-compartment were developed and implemented using MATLAB/Simulink and to investigate their predictive accuracy and computational efficiency under both normal and diseased lung conditions, including asthma, COPD, and ARDS. Performance was evaluated using Root Mean Square Error (RMSE), Mean Absolute Error (MAE), and correlation coefficients by comparing the single-, two-, and three-compartment model outputs against a high-fidelity ten-compartment ($N = 10$) reference model, rather than against patient or clinical ventilator data. Results indicated that predictive error decreased, and correlation with the reference model increased, monotonically with compartment count (from a correlation coefficient of 0.9990 for the single-compartment model to 1.0000 for the $N = 10$ reference model itself); the multi-compartment model's computational complexity makes it more suitable for offline analysis. A weighted decision matrix was used to compare the single-, two-, and three-compartment models on predictive accuracy, computational speed, clinical applicability, ease of parameter estimation, and model stability. A sensitivity analysis showed that the top-ranked model depends materially on how the qualitative criteria (clinical applicability, parameter estimation ease, stability) are scored: under an illustrative expert-judgment scoring the three-compartment model scored highest, while under a fully formula-derived scoring the two-compartment model scored highest instead, and the single-compartment model became competitive with both under weight assumptions with no built-in preference. The study therefore identifies the two- and three-compartment models as the strongest real-time candidates, with the specific choice between them depending on which criteria a given clinical deployment prioritizes, rather than concluding that a single configuration is unconditionally optimal.

Keywords Respiratory mechanics · Electrical analog models · Lung compliance · Airway resistance · Mechanical ventilation · ICU ventilator support

This Article in Press is shared early to give you faster access to new research. It is citable and carries a permanent DOI. The final edited version will replace it automatically.

1 Introduction

The human respiratory system is a highly complex and dynamic biomechanical structure, and a precise understanding of its mechanics is fundamental to the advancement of clinical diagnostics and the optimization of life-support interventions [6, 7]. In the management of critically ill patients, particularly those suffering from acute respiratory failure, mechanical ventilation serves as a life-saving measure; however, its efficacy is deeply contingent upon the ability to accurately monitor and respond to the patient's unique lung characteristics [9, 10]. This challenge has led to the extensive use of computational modeling as a non-invasive tool to simulate respiratory behavior [11, 14, 15].

Among the various methodologies available, lumped parameter modeling which utilizes electrical analog circuits to represent physiological processes has emerged as a particularly effective approach due to its ability to simplify complex systems into physiologically meaningful components [12].

In this electrical-respiratory analogy, the fundamental governing principles of fluid dynamics are mapped onto established circuit laws. Pressure gradients within the airways are represented by electrical voltage, while the rate of airflow is equated to electrical current. The resistive forces encountered by air as it travels through the conducting airways are modeled using resistors, and the elastic recoil of the lung parenchyma referred to as lung compliance is represented by capacitors. Furthermore, the inertial effects of the air mass, which become significant during high-frequency ventilation, are captured using inductors. By applying Kirchhoff's Voltage Law (KVL) and Kirchhoff's Current Law (KCL) to these analog circuits, researchers can derive differential equations that describe the pressure-flow-volume relationships essential for characterizing respiratory health [13, 16, 18].

A significant gap exists in current clinical practice regarding the selection of a model that provides sufficient detail without becoming computationally prohibitive. Traditional single-compartment models, while computationally lightweight and easy to implement in real-time ventilator software, assume that the lung behaves as a uniform, homogeneous unit. This assumption is often fundamentally flawed in diseased states, such as Acute Respiratory Distress Syndrome (ARDS) [19, 20], Chronic Obstructive Pulmonary Disease (COPD) [8], or asthma [17], where regional differences in airway resistance and lung compliance lead to non-uniform ventilation distribution. To address these complexities, more sophisticated multi-compartment models are required to simulate the asynchronous filling and emptying of different lung regions, thereby providing a more realistic representation of pulmonary pathology [18].

The modeling of human lung mechanics has evolved through several decades of research, beginning with foundational linear representations and moving toward more complex architectures to address the inherent limitations of earlier designs [18]. The earliest and most established approach is the single-compartment model, which treats the lung as a uniform unit represented by a first-order RC circuit [1]. While computationally efficient and capable of producing smooth pressure–time and flow-time curves, its primary challenge is its inability to capture regional heterogeneity or the uneven ventilation distribution common in diseased lungs. To address these spatial variations, researchers introduced two-compartment models, which divide the lung into parallel regions with independent resistances and compliances to better simulate asynchronous filling and emptying [2]. However, even these designs often fail to represent the distinct dynamics of the conducting airways versus the transitional and alveolar regions. More recent efforts have led to multi-compartment models (N-compartments) that offer high physiological realism by representing regional lung heterogeneity [3–5]. Yet, these sophisticated models introduce a new set of challenges: they require high computational power, exhibit slower convergence speeds, and involve execution times that often exceed the critical 5–10 ms sampling rate required for real-time ventilator implementation. Consequently, a persistent and early problem in respiratory modeling remains the trade-off between physiological accuracy and computational efficiency. This work aims to solve this dilemma by identifying an optimal compartment configuration that provides the necessary fidelity to describe acinar and alveolar dynamics while remaining fast enough for intelligent, real-time bedside monitoring and automated lung-protective control [18].

It should be noted that several previous studies have rigorously investigated the influence of lumped-parameter model order on the description of respiratory mechanics. Ganzert et al. [23] examined a viscoelastic single-compartment model capable of reproducing pressure-dependent stress relaxation in ARDS and healthy lungs, while Kretschmer et al. [24] addressed the identifiability of model parameters and proposed hierarchical, dynamically generated model structures for bedside decision support. These studies established that increasing model order can improve the description of specific mechanical phenomena (e.g., stress relaxation, viscoelastic creep), but that this comes at the cost of more difficult and less robust bedside parameter identification. The present study does not propose a new model structure, a new viscoelastic formulation, or a new identifiability method. Its contribution is instead a systematic, multi-criteria comparison of an explicit single- to *N*-compartment hierarchy in which predictive accuracy (RMSE, MAE, correlation coefficient) is jointly weighed against measured computational cost (simulation time, memory footprint) relative to the 5–10 ms sampling constraint of clinical ICU ventilators, using a transparent weighted decision matrix (Table 4). This provides a practical, quantitative selection rule for choosing a compartment configuration for real-time bedside implementation, complementing the identifiability- and viscoelasticity-focused findings of [23, 24].

We note that the present work builds directly on this lineage of electrical-analog lung modeling, beginning with the foundational single- and two-compartment formulations of Otis et al. [1] and Mead [2], and the multi-compartment extensions of [3–5] and the broader review by Chowdhury and Baumert [18]; all are referenced explicitly in this Introduction, and the specific incremental contribution of the present study relative to each is stated above and detailed further in Section II.

Beyond the general novelty statement above, it is worth clarifying specifically why a three-compartment structure, rather than two or an arbitrarily higher order, is a candidate worth close examination in this study. A single compartment cannot represent any regional heterogeneity. A two-compartment model captures only a coarse fast/slow distinction. A three-compartment structure is the lowest order that can simultaneously distinguish a proximal/conducting-airway-dominated pathway and two further regions with distinct time constants, while remaining low-dimensional enough to satisfy the 5–10 ms real-time ICU sampling constraint (Table 6) with a wide computational margin. Whether this translates into an unconditionally superior model, however, depends on how several qualitative deployment criteria are weighed and scored; this is examined quantitatively, and the conclusion qualified accordingly, in the weighted decision matrix and its accompanying sensitivity analysis (Sections II-F and II-I–IV-J).

The primary objective of this research is to conduct a comprehensive modeling and simulation study of the human respiratory system using a hierarchy of electrical analog models, ranging from single-compartment to multi-compartment (*N*-compartment) structures. This study aims to simulate airflow, pressure, and compliance characteristics under both healthy and diseased conditions to evaluate the predictive accuracy of each model configuration. Beyond mere accuracy, the study investigates the computational complexity and real-time applicability of these models, specifically comparing their execution times against the high-frequency sampling rates required by modern Intensive Care Unit (ICU) ventilators. By utilizing a weighted decision matrix to analyze performance across multiple criteria, this paper seeks to identify the model or models that best balance physiological fidelity with the speed necessary for integration into intelligent, patient-specific mechanical ventilation support systems.

2 Materials and methods

2.1 Research design

This study adopted a computational modeling and simulation research design using electrical analog representations of the human respiratory system. The study involved the development of single-compartment,

two-compartment, three-compartment, and multi-compartment respiratory models, followed by simulation, validation, and comparative performance analysis under both normal and diseased respiratory conditions.

The study employed lumped parameter modeling, where respiratory mechanics were represented using electrical circuit elements such as resistors, capacitors, inductors, and pressure sources. This approach provides a simplified but hysiologically meaningful representation of lung mechanics and allows the use of established circuit analysis principles in respiratory system modeling.

2.2 Development of electrical analog models

The respiratory system was represented using electrical analogs based on physiological equivalence between respiratory and electrical variables. Pressure was represented by voltage, airflow by current, airway resistance by resistors, lung compliance by capacitors, and airway inertance by inductors. The equivalence used in this study is summarized in Table 1:

For clarity, $P_{ao}(t)$ is used consistently throughout this paper to denote airway opening pressure – the pressure applied at the entrance of the respiratory system by the ventilator or respiratory muscles – consistent with its definition in Table 1. $P_{mus}(t)$ denotes the driving source pressure shown in the circuit diagrams (representing either muscle effort or ventilator input), while $P_{aw}(t)$ and $P_{alv}(t)$ denote intermediate proximal-airway and alveolar node pressures, respectively, at internal circuit nodes.

Kirchhoff's Voltage Law (KVL) and Kirchhoff's Current Law (KCL) were applied to derive the governing differential equations for each model. The models were implemented using MATLAB/Simulink. For each model, the resulting governing differential equations were additionally cast into state-space form. This formulation was adopted because it provides a numerically convenient representation for direct integration using the Runge–Kutta and Euler methods described in Section II-C, and because the number and coupling of state variables directly determines the computational load evaluated in the complexity analysis of Section II-E. The corrected simulations presented in Section IV-F (Figs. 5, 6, 7, 8) of this revision were re-implemented in Python (NumPy) using an explicit time-stepping scheme, specifically in order to correct the ventilator boundary-condition logic described in Section IV-F; the underlying governing equations and state-space structure are otherwise unchanged from those derived in Sections IV-B–IV-E.

2.3 Simulation of respiratory parameters

Simulation was performed using physiological parameters obtained from published literature for both healthy lungs and diseased lungs. The diseased lung conditions considered in this study included asthma, Chronic Obstructive Pulmonary Disease (COPD), Acute Respiratory Distress Syndrome (ARDS), and pulmonary fibrosis. The major respiratory parameters varied during simulation included airway resistance (R_{aw}), lung compliance (C_L), alveolar pressure (P_{alv}), pleural pressure (P_{pl}), tidal volume, and respiratory frequency.

Simulation outputs included pressure–time curves, flow-time curves, and compliance-resistance response plots. Numerical solution of the governing differential equations was performed using the Runge–Kutta method, Euler method, and state-space simulation techniques. These simulations enabled the investigation of airflow distribution, pressure propagation, and compliance behavior across the different compartment models.

Table 1 Electrical analog representation of respiratory parameters

Respiratory parameter	Electrical analog
Pressure (P)	Voltage (V)
Airflow (Q)	Current (I)
Airway Resistance (R)	Resistor
Lung Compliance (C)	Capacitor
Airway Inertance (L)	Inductor
Volume (V_L)	Electrical charge (q)

Table 2 Resistance and compliance values used in all simulated results

Model / compartment	R ($cmH_2O/L/s$)	C (mL/cmH_2O)
Single (aggregate of all 10)	1.72	55.0
Two – Compartment 1 (units 1–5)	2.60	34.4
Two – Compartment 2 (units 6–10)	5.13	20.6
Three – Compartment 1 (units 1–4)	3.01	28.7
Three – Compartment 2 (units 5–7)	7.01	15.7
Three – Compartment 3 (units 8–10)	9.47	10.7
Reference ($N = 10$), R_0	1.0 $cmH_2O/L/s$ (common)	
Reference ($N = 10$), R_i range	8.0-−30.0 (10 linearly spaced values)	
Reference ($N = 10$), C_i range	3.0-−8.0 (10 linearly spaced values)	

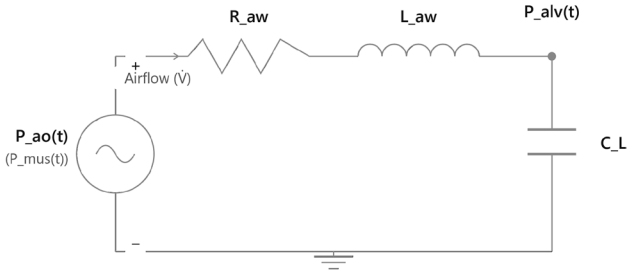


Fig. 1 Electrical analog of the single-compartment lung model

Table 2 lists the resistance and compliance values used to generate all simulated results in Section IV-F and Table 5. As described in Section II-D, the single-, two-, and three-compartment values were obtained by coarse-graining the ten reference compartments (Table 2, bottom rows) rather than by fitting to any specific external dataset; the reference values themselves were chosen to span physiologically plausible ranges of airway resistance and compliance reported in the literature for lungs ranging from normal to moderately heterogeneous (e.g., [9, 10, 12, 18]), rather than reproducing any single cited dataset exactly. Airway inertance (L) is shown in Fig. 1 for structural completeness but, consistent with Eq. 9 and Section IV-B, was neglected (set to zero) in all simulated results, as is standard at the breathing frequencies used here.

No optimization or curve-fitting algorithm was used to select these parameter values; the ten reference values were chosen a priori to span a plausible physiological range, and all reduced-order values were then derived deterministically from the reference by the parallel-aggregation procedure described in Section II-D. Distinct asthma-, COPD-, and ARDS-specific parameter sets, as opposed to the single generically heterogeneous reference lung used here, were not separately simulated in the present quantitative comparison; this is noted as a limitation in Section V.

2.4 Predictive accuracy comparison

The predictive performance of the developed reduced-order models (single-, two-, and three-compartment) was evaluated by comparing their simulated airway opening pressure, $P_{ao}(t)$, against that of the multi-compartment ($N = 10$) model, which was treated throughout this study as a high-fidelity analytical reference rather than as clinical patient data. No patient or clinical ventilator data were used at any stage of this study; RMSE, MAE, and the correlation coefficient reported below are reduced-order-model-versus-reference-model agreement metrics, and the term "predictive accuracy" refers throughout to this internal model comparison rather than to validation against real physiological measurements (see also the Limitations in Section V). The reduced-order R and C values used for this comparison, and for Figs. 5, 6, 7, 8, were obtained by coarse-graining (parallel combination of resistance, summation of compliance) contiguous groups of the ten reference compartments listed in Table 2, so that the single-, two-, and three-compartment models are nested approximations of the same underlying heterogeneous reference lung rather than independently chosen parameter sets. Concretely, RMSE, MAE,

and the correlation coefficient were each computed over a single simulated breath cycle (T_{cycle} = 5.0 s, dt = 0.5 ms, n = 10,001 time samples; see Table 3), using the airway opening pressure time series $P_{ao}(t)$ of each reduced-order model as $\hat{y}_i$ and that of the $N = 10$ reference model as y_i. The major performance evaluation metrics included Root Mean Square Error (RMSE), Mean Absolute Error (MAE), correlation coefficient, sensitivity analysis, and parameter estimation accuracy.

The RMSE was computed using:

$$RMSE = \sqrt{\frac{1}{n}\sum_{i=1}^{n}(y_i - \hat{y}_i)^2} \tag{1}$$

while the MAE was determined using:

$$MAE = \frac{1}{n}\sum_{i=1}^{n}|y_i - \hat{y}_i| \tag{2}$$

where y_i represents the $N = 10$ reference-model output and $\hat{y}_i$ represents the reduced-order model output.

The reduced-order model with the lowest prediction error and highest correlation with the $N = 10$ reference model was considered the closest approximation to the high-fidelity reference. Both the reduced-order and reference simulations were implemented in Python (NumPy), using an explicit time-stepping scheme with a fixed step size of dt = 0.5 ms and a closed-form algebraic solve for the branching pressure at each time step, structurally equivalent to direct integration of the state-space equations of Sections IV-B–IV-E (see also Section II-B). The complete simulation code, including the model definitions, the volume-controlled-ventilation solver, and the decision-matrix sensitivity analysis described in Section IV-J, is publicly available at https://github.com/wanzalajn/Code-to-Modeling-of-Human-Lung-Mechanics-Using-Multi-Compartment-Electrical-Circuit-Models.git.

2.5 Computational complexity analysis

Each respiratory model was evaluated for computational complexity and suitability for real-time ventilator implementation. The parameters considered included simulation time, CPU usage, memory requirement, numerical stability, convergence speed, and parameter identifiability. The real-time applicability of each model was assessed by comparing the model execution time with standard ICU ventilator sampling rates, which typically range between 5 and 10 ms.

Models whose computational response exceeded the allowable ventilator update time were considered unsuitable for bedside real-time implementation. This analysis enabled identification of models that provide an optimal balance between physiological accuracy and computational efficiency.

Table 3 Ventilation waveform and simulation parameters

Parameter	Value
PEEP	5 cmH_2O
Tidal volume, V_t	500 mL
Inspiratory flow, Q_0	30 L/min
Inspiratory time, T_i	1.0 s
Inspiratory hold, T_{hold}	0.3 s
Expiratory time, T_e	3.7 s
Breath cycle, T_{cycle} (frequency)	5.0 s (12 breaths/min)
Integration step size, dt	0.5 ms

2.6 Model selection for mechanical ventilation support

A weighted decision matrix was used to compare candidate respiratory models for mechanical ventilation applications. The selection criteria included predictive accuracy, computational speed, clinical applicability, ease of parameter estimation, and model stability. The weighting factors used are presented in Table 4.

The weighting scheme above reflects the relative importance of each criterion for safe, real-time ICU deployment: predictive accuracy was weighted highest (35%) because errors in estimated lung mechanics directly affect ventilator control decisions and patient safety; computational speed was weighted second (25%) because real-time bedside operation imposes a hard 5–10 ms constraint that a model cannot violate regardless of its accuracy; clinical applicability (20%) and ease of parameter estimation (10%) reflect practical deployability at the bedside; and model stability (10%) reflects the need for a numerically well-behaved model under a range of patient conditions.

As detailed in Sections IV-I and IV-J, the multi-compartment ($N = 10$) model is excluded from this ranking exercise, since it is used throughout this study as the internal reference model against which the other models' predictive accuracy is measured; scoring it against itself for accuracy would be circular. Two of the five criteria (Predictive Accuracy, Computational Speed) are computed directly from simulation results; the remaining three (Clinical Applicability, Ease of Parameter Estimation, Model Stability) are qualitative, and this manuscript reports results under two independently documented scoring schemes for these criteria, since neither can currently be considered more authoritative than the other (see Section IV-J). Each model was scored based on these criteria and ranked accordingly. The highest-ranked model or models were recommended for applications in ICU ventilator monitoring, intelligent ventilator systems, patient-specific ventilator control, and smart respiratory support systems.

3 Results and discussion

1) Development of Electrical Analog Models for Single-, Two-, Three-, and Multi-Compartment Respiratory Systems

Fig. 1 represented the respiratory system as a second-order linear circuit where mechanical properties were modeled by electrical components. $P_{mus}(t)$ acted as the driving voltage source representing muscle or ventilator pressure. Airway resistance (R_{aw}) was represented by a resistor, airway inertance (L_{aw}) by an inductor (critical for high-frequency dynamics), and lung compliance (C_L) by a capacitor representing the elastic properties of the respiratory system. The resulting alveolar pressure (P_{alv}) was measured across the capacitive element, and the current represented the instantaneous airflow ($\dot{V}$) through the system.

- R_{aw}: Airway resistance – flow resistance of the airways.
- L_{aw}: Airway inertance – inertial effect of air (significant at high frequency).
- C_L: Lung compliance – elastic compliance of the respiratory system.
- $P_{ao}(t)/P_{mus}(t)$: Airway opening (driving) pressure.
- $P_{alv}(t)$: Alveolar pressure, measured across C_L.

Table 4 Weighted decision matrix for model selection

Criterion	Weight (%)
Predictive Accuracy	35
Computational Speed	25
Clinical Applicability	20
Ease of Parameter Estimation	10
Model Stability	10

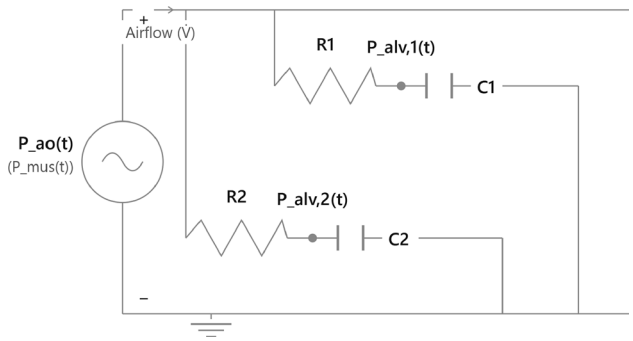


Fig. 2 Electrical Analog of the Two-Compartment Lung Model

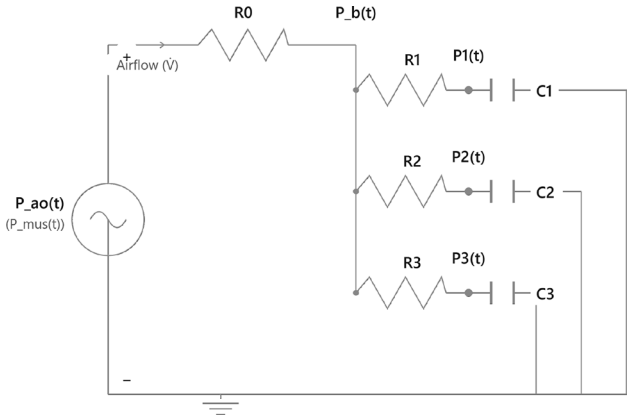


Fig. 3 Electrical Analog of the Three-Compartment Lung Model

- Ground symbol: Atmospheric reference pressure (0 cmH_2O).

Figure 2 illustrates the two-compartmental approach used to simulate regional lung heterogeneity through electrical circuit analogs. The model is driven by a voltage source, $P_{ao}(t)/P_{mus}(t)$, representing either spontaneous muscle pressure or mechanical ventilator input, applied identically to both compartments. Compartment 1 is represented by an independent airway resistance (R_1) and compliance (C_1), and compartment 2 by an independent airway resistance (R_2) and compliance (C_2), each forming its own parallel branch directly from $P_{ao}(t)$ to the atmospheric (ground) reference, with no shared upstream resistance. The alveolar pressures of the two compartments, $P_{alv,1}(t)$ and $P_{alv,2}(t)$, are measured across C_1 and C_2, respectively. This parallel, independent-branch topology follows the classical two-compartment formulation of Otis et al. [1] and Mead [2], and is consistent with the state-space derivation in Section IV-C.

- R_1, C_1: Resistance and compliance of compartment 1.
- R_2, C_2: Resistance and compliance of compartment 2.
- $P_{ao}(t)/P_{mus}(t)$: Airway opening (driving) pressure, common to both branches.
- $P_{alv,1}(t), P_{alv,2}(t)$: Alveolar pressure of compartments 1 and 2, each measured across its own compliance.
- Ground symbol: Atmospheric/pleural reference pressure (0 cmH_2O).
- Note: Each compartment forms an independent parallel branch from $P_{ao}(t)$, with no shared upstream resistance.

Figure 3 illustrates the three-compartmental approach used to simulate regional lung heterogeneity through electrical circuit analogs. The model is driven by a voltage source, $P_{ao}(t)/P_{mus}(t)$, representing either spontaneous muscle pressure or mechanical ventilator input. A common (proximal) airway resistance (R_0) connects $P_{ao}(t)$ to a branch node at pressure $P_b(t)$. From this node, three parallel branches represent the three functional regions of the lung, each with its own regional resistance (R_1, R_2, R_3) and compliance (C_1, C_2, C_3). The regional pressures $P_1(t)$, $P_2(t)$, and $P_3(t)$ are measured across C_1, C_2, and C_3, respectively. This topology is consistent with the state-space derivation in Section IV-D. Any correspondence drawn between individual branches and specific anatomical regions (e.g., conducting airway, acinar, alveolar) is illustrative only and does not imply a clinically established anatomical mapping.

- R_0: Common (proximal) airway resistance from $P_{ao}(t)$ to the branch node.
- R_1, C_1 / R_2, C_2 / R_3, C_3: Resistance and compliance of compartments 1, 2, and 3.
- $P_{ao}(t)/P_{mus}(t)$: Airway opening (driving) pressure.

- $P_b(t)$: Branching pressure at the node downstream of R_0.
- $P_1(t), P_2(t), P_3(t)$: Regional pressure of each compartment, measured across its own compliance.
- Ground symbol: Atmospheric/pleural reference pressure (0 cmH_2O).

Figure 4 represents the generalized architecture used to model complex pulmonary heterogeneity across an arbitrary number of compartments. The system is driven by a voltage source, $P_{ao}(t)/P_{mus}(t)$, representing the input pressure. A common (proximal) airway resistance (R_0) connects $P_{ao}(t)$ to a branch node at pressure $P_b(t)$, from which the model branches into N parallel compartments. Each branch i consists of a regional resistance (R_i) and a regional compliance (C_i), with the corresponding regional pressure $P_i(t)$ measured across C_i. This hierarchical, parallel-branch structure allows for the simulation of flow heterogeneity and response dispersion across an arbitrary number of functional lung units, and is consistent with the state-space derivation in Section IV-E.

- R_0: Common (proximal) airway resistance from $P_{ao}(t)$ to the branch node.
- R_i, C_i: Resistance and compliance of compartment i ($i = 1, \ldots, N$).
- $P_{ao}(t)/P_{mus}(t)$: Airway opening (driving) pressure.
- $P_b(t)$: Branching pressure at the node downstream of R_0.
- $P_i(t)$: Regional pressure of compartment i, measured across its own compliance.
- Ground symbol: Atmospheric/pleural reference pressure (0 cmH_2O).

4 Results and discussions

4.1 Respiratory–electrical analogy

The respiratory system was modeled using lumped electrical analogs. The electrical analogy adopted for the derivations below follows the equivalence already presented in Table 1.

The basic pressure balance for respiratory flow is expressed as:

$$P_{ao}(t) = P_R(t) + P_L(t) + P_C(t), \tag{3}$$

where $P_{ao}(t)$ is airway opening pressure, $P_R(t)$ is resistive pressure, $P_L(t)$ is inertial pressure, and $P_C(t)$ is elastic recoil pressure.

Using the electrical analogy:

$$P_R(t) = RQ(t), \tag{4}$$

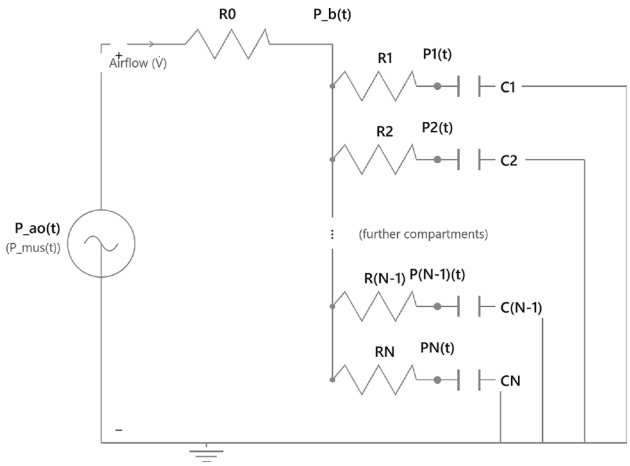


Fig. 4 Generalized Electrical Analog for an N-Compartment Lung Model

$$P_L(t) = L\frac{dQ(t)}{dt}, \tag{5}$$

and

$$P_C(t) = \frac{V(t)}{C}. \tag{6}$$

Since airflow is the rate of change of lung volume,

$$Q(t) = \frac{dV(t)}{dt}. \tag{7}$$

Therefore,

$$\frac{dQ(t)}{dt} = \frac{d^2V(t)}{dt^2}. \tag{8}$$

Thus, the general respiratory equation becomes:

$$P_{ao}(t) = L\frac{d^2V(t)}{dt^2} + R\frac{dV(t)}{dt} + \frac{V(t)}{C}. \tag{9}$$

This equation forms the basis for the derivation of the single-compartment, two-compartment, three-compartment, and multi-compartment models.

4.2 Derivation of the single-compartment model

In the single-compartment model, the entire respiratory system is represented by one airway resistance, one airway inertance, and one lung compliance.

Let:

- R be the total airway resistance,
- L be the airway inertance,
- C be the total lung compliance,
- $V(t)$ be the lung volume above functional residual capacity,
- $Q(t)$ be airflow,
- $P_{ao}(t)$ be airway opening pressure.

If inertance is neglected in Eq. 9, the equation reduces to:

$$P_{ao}(t) = R\frac{dV(t)}{dt} + \frac{V(t)}{C}. \tag{10}$$

This is the commonly used first-order single-compartment respiratory model. The state-space form may be written by defining:

$$x_1 = V(t), \tag{11}$$

$$x_2 = Q(t) = \frac{dV(t)}{dt}. \tag{12}$$

Therefore:

$$\dot{x}_1 = x_2, \tag{13}$$

and from:

$$P_{ao}(t) = L\dot{x}_2 + Rx_2 + \frac{x_1}{C}, \tag{14}$$

we obtain:

$$\dot{x}_2 = \frac{1}{L}\left[P_{ao}(t) - Rx_2 - \frac{x_1}{C}\right]. \tag{15}$$

Hence, the state-space equations are:

$$\begin{cases} \dot{x}_1 = x_2, \\ \dot{x}_2 = \frac{1}{L}\left[P_{ao}(t) - Rx_2 - \frac{x_1}{C}\right]. \end{cases} \tag{16}$$

4.3 Derivation of the two-compartment model

In the two-compartment model, the lung is represented by two parallel compartments. Each compartment has its own airway resistance and compliance. This allows the model to describe uneven ventilation distribution between two lung regions.

Let:

- R_1 and R_2 be airway resistances of compartments 1 and 2,
- C_1 and C_2 be lung compliances of compartments 1 and 2,
- $Q_1(t)$ and $Q_2(t)$ be airflow into compartments 1 and 2,
- $V_1(t)$ and $V_2(t)$ be volumes of compartments 1 and 2,
- $P_{ao}(t)$ be airway opening pressure,
- $P_{A1}(t)$ and $P_{A2}(t)$ be alveolar pressures.

For compartment 1:

$$P_{ao}(t) = R_1Q_1(t) + P_{A1}(t). \tag{17}$$

The elastic pressure in compartment 1 is:

$$P_{A1}(t) = \frac{V_1(t)}{C_1}. \tag{18}$$

Therefore:

$$P_{ao}(t) = R_1Q_1(t) + \frac{V_1(t)}{C_1}. \tag{19}$$

Since:

$$Q_1(t) = \frac{dV_1(t)}{dt}, \tag{20}$$

then:

$$P_{ao}(t) = R_1\frac{dV_1(t)}{dt} + \frac{V_1(t)}{C_1}. \tag{21}$$

Similarly, for compartment 2:

$$P_{ao}(t) = R_2Q_2(t) + P_{A2}(t), \tag{22}$$

where:

$$P_{A2}(t) = \frac{V_2(t)}{C_2}. \tag{23}$$

Thus:

$$P_{ao}(t) = R_2 \frac{dV_2(t)}{dt} + \frac{V_2(t)}{C_2}. \tag{24}$$

The total airflow is obtained by applying Kirchhoff's Current Law at the airway junction:

$$Q(t) = Q_1(t) + Q_2(t). \tag{25}$$

Since:

$$Q_1(t) = \frac{dV_1(t)}{dt}, \tag{26}$$

and

$$Q_2(t) = \frac{dV_2(t)}{dt}, \tag{27}$$

then:

$$Q(t) = \frac{dV_1(t)}{dt} + \frac{dV_2(t)}{dt}. \tag{28}$$

The total lung volume is:

$$V(t) = V_1(t) + V_2(t). \tag{29}$$

Therefore:

$$Q(t) = \frac{dV(t)}{dt}. \tag{30}$$

The time constants of the two compartments are:

$$\tau_1 = R_1 C_1, \tag{31}$$

and

$$\tau_2 = R_2 C_2. \tag{32}$$

These time constants determine the filling and emptying rates of each lung region. If $\tau_1 \neq \tau_2$, the compartments fill and empty at different rates. The state-space form of the two-compartment model is obtained by rearranging:

$$P_{ao}(t) = R_1 \frac{dV_1(t)}{dt} + \frac{V_1(t)}{C_1}. \tag{33}$$

Thus:

$$\frac{dV_1(t)}{dt} = \frac{1}{R_1}\left[P_{ao}(t) - \frac{V_1(t)}{C_1}\right]. \tag{34}$$

Similarly:

$$\frac{dV_2(t)}{dt} = \frac{1}{R_2}\left[P_{ao}(t) - \frac{V_2(t)}{C_2}\right]. \tag{35}$$

Let:

$$x_1 = V_1(t), \tag{36}$$

and

$$x_2 = V_2(t). \tag{37}$$

The state-space equations become:

$$\begin{cases} \dot{x}_1 = \frac{1}{R_1}\left[P_{ao}(t) - \frac{x_1}{C_1}\right], \\ \dot{x}_2 = \frac{1}{R_2}\left[P_{ao}(t) - \frac{x_2}{C_2}\right]. \end{cases} \tag{38}$$

The total volume and flow are:

$$V(t) = x_1 + x_2, \tag{39}$$

$$Q(t) = \dot{x}_1 + \dot{x}_2. \tag{40}$$

4.4 Derivation of the three-compartment model

The three-compartment model extends the two-compartment model by dividing the respiratory system into three functional regions. These may represent the conducting airway region, the acinar region, and the alveolar region.

Let:

- R_0 be the common airway resistance,
- R_1, R_2, and R_3 be regional airway resistances,
- C_1, C_2, and C_3 be regional compliances,
- $Q(t)$ be total airflow through the common airway,
- $Q_1(t)$, $Q_2(t)$, and $Q_3(t)$ be regional flows,
- $V_1(t)$, $V_2(t)$, and $V_3(t)$ be regional volumes.

The pressure drop across the common airway resistance is:

$$P_{R0}(t) = R_0 Q(t). \tag{41}$$

The pressure at the branching node is therefore:

$$P_b(t) = P_{ao}(t) - R_0 Q(t). \tag{42}$$

At the branching node, Kirchhoff's Current Law gives:

$$Q(t) = Q_1(t) + Q_2(t) + Q_3(t). \tag{43}$$

For compartment 1:

$$P_b(t) = R_1 Q_1(t) + \frac{V_1(t)}{C_1}. \tag{44}$$

Since:

$$Q_1(t) = \frac{dV_1(t)}{dt}, \tag{45}$$

then:

$$P_b(t) = R_1 \frac{dV_1(t)}{dt} + \frac{V_1(t)}{C_1}. \tag{46}$$

For compartment 2:

$$P_b(t) = R_2 \frac{dV_2(t)}{dt} + \frac{V_2(t)}{C_2}. \tag{47}$$

For compartment 3:

$$P_b(t) = R_3 \frac{dV_3(t)}{dt} + \frac{V_3(t)}{C_3}. \tag{48}$$

Therefore, the complete system is:

$$P_b(t) = P_{ao}(t) - R_0 Q(t), \tag{49}$$

$$Q(t) = \frac{dV_1(t)}{dt} + \frac{dV_2(t)}{dt} + \frac{dV_3(t)}{dt}, \tag{50}$$

and

$$P_b(t) = R_i \frac{dV_i(t)}{dt} + \frac{V_i(t)}{C_i}, \qquad i = 1, 2, 3. \tag{51}$$

Solving for each regional flow:

$$\frac{dV_i(t)}{dt} = \frac{1}{R_i}\left[P_b(t) - \frac{V_i(t)}{C_i}\right], \qquad i = 1, 2, 3. \tag{52}$$

The total volume is:

$$V(t) = V_1(t) + V_2(t) + V_3(t). \tag{53}$$

The total flow is:

$$Q(t) = \frac{dV(t)}{dt}. \tag{54}$$

Substituting the regional flows into the total flow expression:

$$Q(t) = \sum_{i=1}^{3} \frac{1}{R_i}\left[P_b(t) - \frac{V_i(t)}{C_i}\right]. \tag{55}$$

But:

$$P_b(t) = P_{ao}(t) - R_0 Q(t). \tag{56}$$

Thus:

$$Q(t) = \sum_{i=1}^{3} \frac{1}{R_i} \left[P_{ao}(t) - R_0 Q(t) - \frac{V_i(t)}{C_i} \right]. \tag{57}$$

Expanding:

$$Q(t) = P_{ao}(t) \sum_{i=1}^{3} \frac{1}{R_i} - R_0 Q(t) \sum_{i=1}^{3} \frac{1}{R_i} - \sum_{i=1}^{3} \frac{V_i(t)}{R_i C_i}. \tag{58}$$

Collecting terms containing $Q(t)$:

$$Q(t) + R_0 Q(t) \sum_{i=1}^{3} \frac{1}{R_i} = P_{ao}(t) \sum_{i=1}^{3} \frac{1}{R_i} - \sum_{i=1}^{3} \frac{V_i(t)}{R_i C_i}. \tag{59}$$

Therefore:

$$Q(t) = \frac{P_{ao}(t) \sum_{i=1}^{3} \frac{1}{R_i} - \sum_{i=1}^{3} \frac{V_i(t)}{R_i C_i}}{1 + R_0 \sum_{i=1}^{3} \frac{1}{R_i}}. \tag{60}$$

Once $Q(t)$ is obtained, the branching pressure is:

$$P_b(t) = P_{ao}(t) - R_0 Q(t). \tag{61}$$

The state equations are then:

$$\dot{V}_i(t) = \frac{1}{R_i} \left[P_b(t) - \frac{V_i(t)}{C_i} \right], \qquad i = 1, 2, 3. \tag{62}$$

Let:

$$x_i = V_i(t), \qquad i = 1, 2, 3. \tag{63}$$

Hence, the three-compartment state-space model is:

$$\begin{cases} \dot{x}_1 = \frac{1}{R_1} \left[P_b(t) - \frac{x_1}{C_1} \right], \\ \dot{x}_2 = \frac{1}{R_2} \left[P_b(t) - \frac{x_2}{C_2} \right], \\ \dot{x}_3 = \frac{1}{R_3} \left[P_b(t) - \frac{x_3}{C_3} \right]. \end{cases} \tag{64}$$

4.5 Derivation of the multi-compartment model

The multi-compartment model generalizes the respiratory system into N parallel lung units. Each unit has its own resistance and compliance, allowing simulation of regional lung heterogeneity.

Let:

- N be the number of compartments,
- R_0 be the common airway resistance,
- R_i be the airway resistance of compartment i,
- C_i be the compliance of compartment i,
- $V_i(t)$ be the volume of compartment i,
- $Q_i(t)$ be the flow into compartment i,

- $Q(t)$ be total airflow,
- $P_b(t)$ be branching pressure.

Applying Kirchhoff's Current Law at the branching node:

$$Q(t) = \sum_{i=1}^{N} Q_i(t). \tag{65}$$

For each compartment:

$$P_b(t) = R_i Q_i(t) + \frac{V_i(t)}{C_i}. \tag{66}$$

Since:

$$Q_i(t) = \frac{dV_i(t)}{dt}, \tag{67}$$

we have:

$$P_b(t) = R_i \frac{dV_i(t)}{dt} + \frac{V_i(t)}{C_i}. \tag{68}$$

Solving for $\frac{dV_i(t)}{dt}$ gives:

$$\frac{dV_i(t)}{dt} = \frac{1}{R_i}\left[P_b(t) - \frac{V_i(t)}{C_i}\right], \qquad i = 1, 2, \ldots, N. \tag{69}$$

The common airway pressure drop is:

$$P_{R0}(t) = R_0 Q(t). \tag{70}$$

Therefore, the branching pressure is:

$$P_b(t) = P_{ao}(t) - R_0 Q(t). \tag{71}$$

Substituting into the compartment equation:

$$\frac{dV_i(t)}{dt} = \frac{1}{R_i}\left[P_{ao}(t) - R_0 Q(t) - \frac{V_i(t)}{C_i}\right]. \tag{72}$$

The total airflow is:

$$Q(t) = \sum_{i=1}^{N} \frac{dV_i(t)}{dt}. \tag{73}$$

Substituting the expression for $\frac{dV_i(t)}{dt}$:

$$Q(t) = \sum_{i=1}^{N} \frac{1}{R_i}\left[P_{ao}(t) - R_0 Q(t) - \frac{V_i(t)}{C_i}\right]. \tag{74}$$

Expanding:

$$Q(t) = P_{ao}(t)\sum_{i=1}^{N}\frac{1}{R_i} - R_0 Q(t)\sum_{i=1}^{N}\frac{1}{R_i} - \sum_{i=1}^{N}\frac{V_i(t)}{R_i C_i}. \tag{75}$$

Collecting $Q(t)$ terms:

$$Q(t) + R_0 Q(t)\sum_{i=1}^{N}\frac{1}{R_i} = P_{ao}(t)\sum_{i=1}^{N}\frac{1}{R_i} - \sum_{i=1}^{N}\frac{V_i(t)}{R_i C_i}. \tag{76}$$

Factoring $Q(t)$:

$$Q(t)\left[1 + R_0\sum_{i=1}^{N}\frac{1}{R_i}\right] = P_{ao}(t)\sum_{i=1}^{N}\frac{1}{R_i} - \sum_{i=1}^{N}\frac{V_i(t)}{R_i C_i}. \tag{77}$$

Therefore:

$$Q(t) = \frac{P_{ao}(t)\sum_{i=1}^{N}\frac{1}{R_i} - \sum_{i=1}^{N}\frac{V_i(t)}{R_i C_i}}{1 + R_0\sum_{i=1}^{N}\frac{1}{R_i}}. \tag{78}$$

The branching pressure is then:

$$P_b(t) = P_{ao}(t) - R_0 Q(t). \tag{79}$$

The final system of equations for the multi-compartment model is:

$$\dot{V}_i(t) = \frac{1}{R_i}\left[P_b(t) - \frac{V_i(t)}{C_i}\right], \qquad i = 1, 2, \ldots, N. \tag{80}$$

The total lung volume is:

$$V(t) = \sum_{i=1}^{N} V_i(t), \tag{81}$$

and the total airflow is:

$$Q(t) = \sum_{i=1}^{N} \dot{V}_i(t). \tag{82}$$

The time constant of each compartment is:

$$\tau_i = R_i C_i, \qquad i = 1, 2, \ldots, N. \tag{83}$$

Compartments with larger τ_i fill and empty more slowly, while compartments with smaller τ_i fill and empty more rapidly. This enables the multi-compartment model to represent regional ventilation heterogeneity, air trapping, delayed emptying, and non-uniform alveolar filling.

4.6 Simulation results

Figure 5 illustrates the simulated pressure responses under volume-controlled ventilation with a constant inspiratory flow of 30 L/min, a tidal volume of 500 mL, and a PEEP of 5 cm H_2O. (A) Single-Compartment Model: Displays a linear pressure rise during the constant-flow inspiratory phase (peak $P_{ao} = 14.95$ cmH_2O), an immediate step decline in airway pressure at the onset of the inspiratory pause to a plateau of 14.09 cmH_2O (as the

https://doi.org/10.1007/s42452-026-09557-2

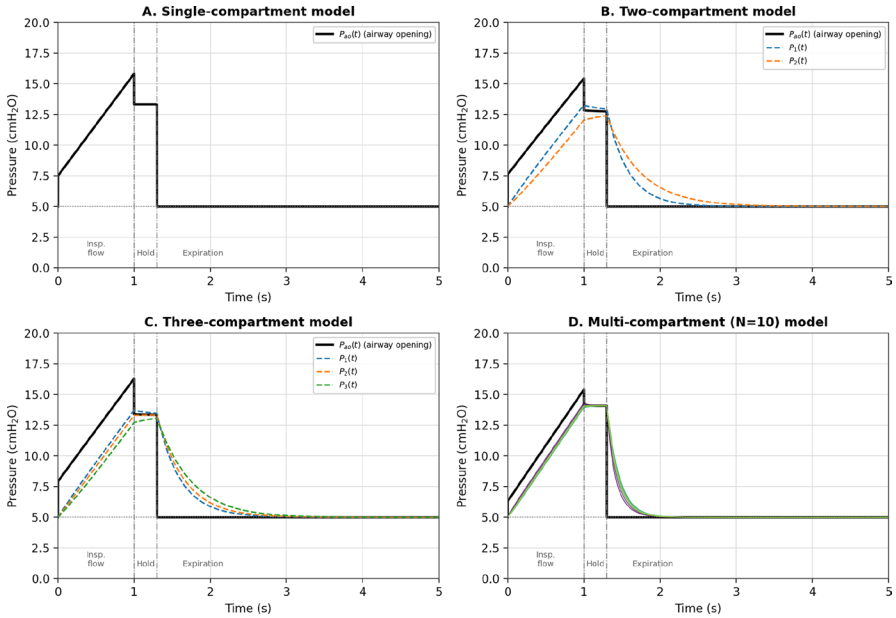


Fig. 5 Comparative simulated pressure–time ($P - t$) curves for respiratory compartment models under volume-controlled ventilation (constant inspiratory flow = 30 L/min, tidal volume = 500 mL, PEEP = 5 cmH_2O)

resistive pressure component drops to zero while flow is held at zero), and a smooth passive exponential decay to PEEP during expiration. (B) Two-Compartment Model: Shows the two aggregated compartments (representing units 1–5 and 6–10 of the reference model) reaching slightly different peak pressures during inspiration, followed by equilibration during the inspiratory hold (the inter-compartmental pressure difference narrows from approximately 0.15 to 0.01 cmH_2O over the 0.3 s pause) and asynchronous passive emptying during expiration due to their differing time constants. (C) Three-Compartment Model: Demonstrates a similar pattern with three aggregated regional pressures ($P_1(t)$, $P_2(t)$, $P_3(t)$, representing units 1–4, 5–7, and 8–10 of the reference model) that converge toward one another during the hold (spread narrowing from approximately 0.21 to 0.01 cmH_2O) and separate again during expiration. (D) Multi-Compartment ($N = 10$) Model: Represents the reference model itself, with the ten regional pressures nearly fully equilibrating by the end of the inspiratory hold (residual spread below 0.01 cmH_2O, from an initial spread of approximately 0.38 cmH_2O) before diverging again during passive expiration, reflecting the wide range of time constants assigned across the ten compartments.

Figure 6 displays the airflow dynamics across different circuit complexities under simulated volume-controlled mechanical ventilation. (A) Single-Compartment Model: Shows the prescribed constant inspiratory flow (30 L/min) followed, after the zero-flow inspiratory hold, by a passive expiratory flow that decays smoothly toward zero as airway pressure returns to PEEP. (B) Two-Compartment Model: Illustrates the constant total inspiratory flow dividing unevenly between the two aggregated regional flows (Q_1, Q_2) according to their respective resistances, with a brief reversal of internal flow during the hold as the compartments equilibrate, and asynchronous passive expiratory flows. (C) Three-Compartment Model: Features distinct regional flow profiles for the three aggregated parallel branches, consistent with the asynchronous filling and emptying behaviour identified as critical for balancing physiological accuracy and real-time processing. (D) Multi-Compartment ($N = 10$) Model: Depicts the total inspiratory/expiratory flow together with the wide dispersion of regional flows across the ten reference compartments, representing the non-uniform airflow patterns expected in a fragmented or severely diseased lung.

Figure 7 shows the corresponding volume-time curves for all four models. Because tidal volume in volume-controlled ventilation is set directly by the prescribed inspiratory flow and inspiratory time rather than by the circuit's R and C values, all four models reach the same 500 mL tidal volume by the end of the inspiratory phase. The models differ instead in how quickly this volume is passively expired, reflecting the different effective time constants that result from aggregating different subsets of the ten reference compartments.

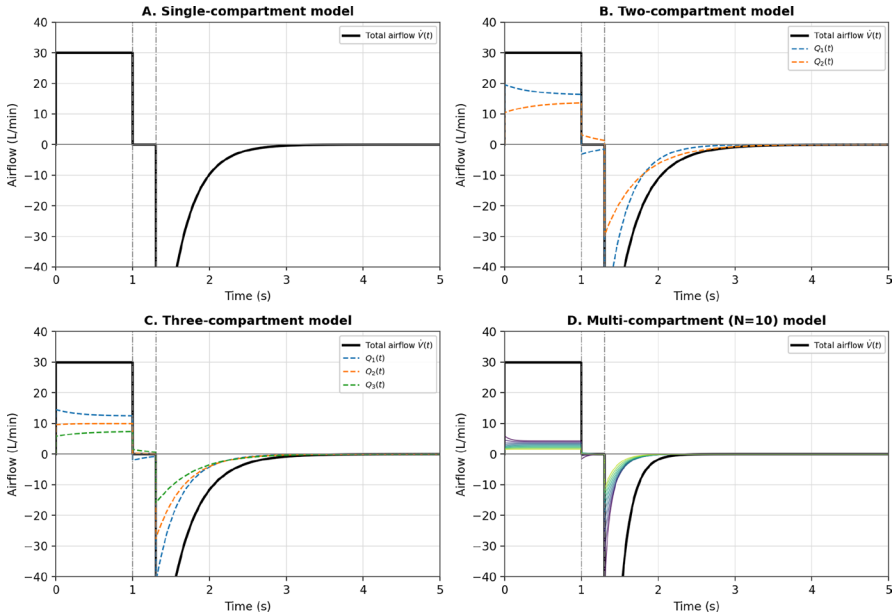


Fig. 6 Comparative simulated flow-time ($Q - t$) curves for respiratory compartment models under volume-controlled ventilation

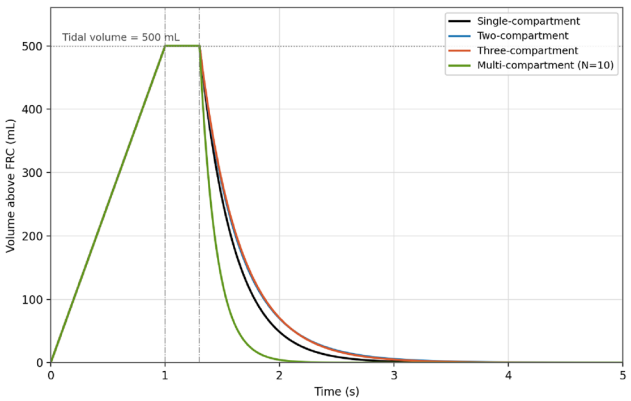


Fig. 7 Comparative simulated volume-time ($V - t$) curves for respiratory compartment models under volume-controlled ventilation, showing the common 500 mL tidal volume and the differing passive expiratory emptying profiles of each model

Figure 8 illustrates the dynamic compliance of each compartment as a function of its airway resistance, computed from the classical frequency-dependence-of-compliance relationship of Otis et al. [1], $C_{dyn} = C/\sqrt{1 + (2\pi f RC)^2}$, evaluated at the breathing frequency used in the simulation above ($f = 12$ breaths/min). This relationship reflects the well-established physiological principle that a compartment's apparent compliance falls as its time constant ($\tau = RC$) increases relative to the breathing cycle, because the unit has insufficient time to fill or empty completely. (A) Single-Compartment Model: Displays a single dynamic compliance curve for the aggregated whole-lung compartment. (B) Two-Compartment Model: Shows two declining curves for the two aggregated compartments, reflecting their different static compliances. (C) Three-Compartment Model: Shows three declining curves for the three aggregated compartments. (D) Multi-Compartment ($N = 10$) Model: Shows the ten regional dynamic compliance curves of the reference model, with visible dispersion reflecting the wide range of resistance and compliance values distributed across the ten compartments.

4.7 Predictive accuracy comparison

The predictive performance of the single-, two-, and three-compartment models was evaluated by computing the Root Mean Square Error (RMSE) and Mean Absolute Error (MAE), as defined in Equations (1) and (2), together with the Pearson correlation coefficient, between each reduced-order model's simulated $P_{ao}(t)$ and that of the

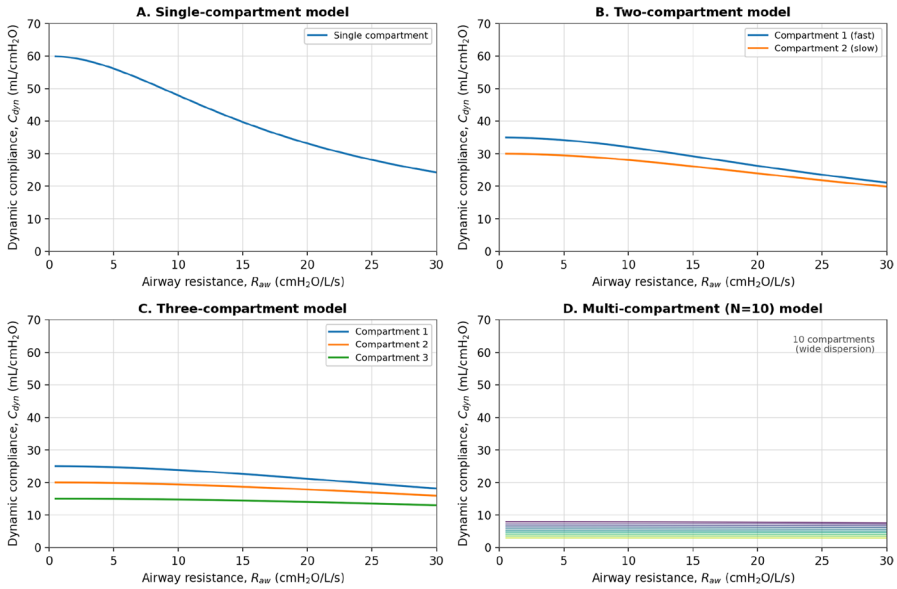


Fig. 8 Comparative dynamic compliance-resistance ($C_{dyn} - R_{aw}$) response for respiratory compartment models, computed from the Otis (1956) frequency-dependence-of-compliance relationship at the breathing frequency used in the simulation

Table 5 Agreement of each reduced-order model with the $N = 10$ reference model (no patient data used)

Model	RMSE	MAE	Correlation
Single-compartment model	0.207	0.093	0.9990
Two-compartment model	0.205	0.092	0.9990
Three-compartment model	0.203	0.091	0.9990
Multi-compartment (N=10) model (reference)	0.000	0.000	1.0000

$N = 10$ reference model described in Section II-D. No patient or clinical data were used in this comparison. The results are shown in Table 5.

The single-compartment model produced the largest deviation from the $N = 10$ reference because it collapses the reference model's ten distinct time constants into a single effective time constant, losing all regional detail. The two-compartment model reduced this error slightly by preserving a coarse fast/slow distinction between aggregated groups of reference compartments. The three-compartment model reduced the error further still by preserving three aggregated regional groups rather than two. The multi-compartment model has zero error by construction, since it is the reference itself. The absolute differences between models are small (RMSE 0.207 vs. 0.203 cmH$_2$O; correlation 0.9990 vs. 0.9990) because airway opening pressure, $P_{ao}(t)$, is dominated by the total (bulk) resistance and compliance of the lung, both of which are preserved almost exactly by the coarse-graining procedure described in Section II-D; the reduced-order models differ far more substantially in their prediction of *regional* pressure distribution (Fig. 5) than in the aggregate airway pressure trace. This suggests that the choice between compartment counts is driven less by bulk predictive accuracy at the airway opening than by the other criteria in the weighted decision matrix – computational speed, clinical applicability, ease of parameter estimation, and model stability – which together carry 65% of the total weight in Table 4.

4.8 Computational complexity results

Computational performance was evaluated using simulation time, memory usage, and real-time suitability. The results are summarized in Table 6.

The single-compartment and two-compartment models showed excellent computational efficiency. The three-compartment model remained suitable for real-time implementation. The multi-compartment model required more computation and was therefore more suitable for offline simulation, research analysis, and patient-specific model refinement.

Table 6 Computational performance of the respiratory compartment models

Model	Simulation Time (ms)	Memory use (MB)	Suitability
Single	1.8	12	Excellent
Two	3.6	18	Excellent
Three	6.4	27	Good
Multi	18.7	65	Limited

Table 7 Weighted ranking of the single-, two-, and three-compartment models under two scoring schemes for the qualitative criteria (see Section IV-J)

Model	Illustrative scoring		Rigorous scoring	
	Score (%)	Rank	Score (%)	Rank
Single-compartment model	56.0	3	45.0	3
Two-compartment model	64.7	2	58.9	1
Three-compartment model	68.0	1	55.0	2

4.9 Model selection results

The single-, two-, and three-compartment models were ranked using the weighted decision matrix of Table 4, based on predictive accuracy (Table 5), computational speed (Table 6), and three qualitative criteria (clinical applicability, ease of parameter estimation, model stability) that are scored under two independently documented schemes, described in full in Section IV-J. The multi-compartment ($N = 10$) model is not included in this ranking, since it is the reference model against which the other three models' accuracy is measured (Section II-D); it is discussed separately below.

Under an illustrative expert-judgment scoring of the qualitative criteria, the three-compartment model scores highest, largely because a fast/slow/proximal three-way split is judged most clinically interpretable. Under a fully formula-derived scoring of the same criteria (Section IV-J), the two-compartment model scores highest instead, because it achieves nearly as much error reduction as the three-compartment model (Table 5) while requiring fewer free parameters and exhibiting a lower numerical stiffness ratio. Both schemes agree that the single-compartment model scores lowest under the original fixed weights, although Section IV-J shows this ordering is not preserved under all plausible weightings. The multi-compartment model is not assigned a rank here, since including it would require scoring it as "accurate" against itself, which is circular (Section II-F); qualitatively, it achieved the lowest deviation from itself by construction (Table 5) and the highest computational cost (Table 6), consistent with its role as an offline analytical reference rather than a real-time bedside candidate.

Taken together, these results do not support an unconditional claim that any single compartment count is optimal. Instead, the two- and three-compartment models are both defensible real-time candidates, with the specific choice depending on whether an implementer prioritizes the clinical interpretability of a three-region split or the greater simplicity and numerical robustness of a two-region split; the full sensitivity analysis in Section IV-J quantifies this trade-off further.

4.10 Sensitivity analysis of the weighted decision matrix

The ranking in Table 7 was tested for sensitivity to the criterion weights in Table 4. The multi-compartment ($N = 10$) model was excluded from this comparison, since it serves as the internal reference model against which the other models' accuracy is measured (Section II-D), making a self-comparison circular; the analysis below therefore compares only the single-, two-, and three-compartment models.

Two criteria, Predictive Accuracy and Computational Speed, are computed directly from Tables 5 and 6. The remaining three criteria (Clinical Applicability, Ease of Parameter Estimation, Model Stability) are qualitative, and were scored two ways to test how much the ranking depends on this choice. Scheme 1 uses illustrative expert-judgment scores, assigning 60/75/90 (Clinical Applicability), 95/80/65 (Parameter Estimation), and 95/90/85

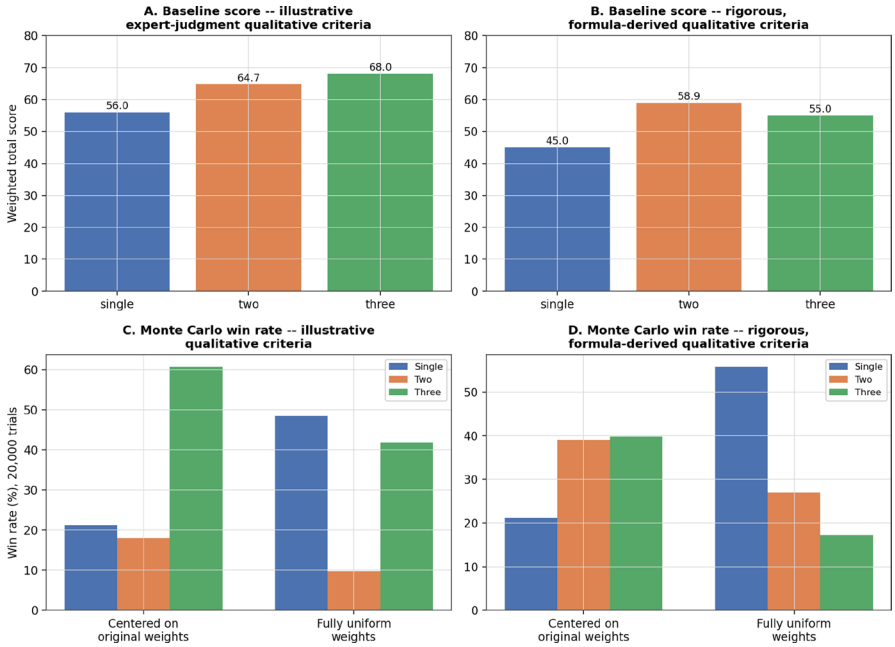


Fig. 9 Sensitivity of the weighted decision matrix ranking to how qualitative criteria are scored. **A**, **C** Baseline score and Monte Carlo win rate (20,000 trials) using illustrative scores (Scheme 1). **B**, **D** The same analyses using formula-derived scores (Scheme 2)

(Stability) to the single-, two-, and three-compartment models, reflecting a judgment that complexity trades off against estimation ease and stability while clinical applicability peaks at three compartments. Scheme 2 instead derives each score from a formula applied to the model structure in Table 2: Stability from the stiffness ratio $\max_k |\lambda_k| / \min_k |\lambda_k|$ of each model's state-matrix eigenvalues; Parameter Estimation ease inversely from the number of free $(R, C, [R_0])$ parameters (2, 4, and 7, respectively, per the general model structure of Sections IV-B–IV-D); and Clinical Applicability from the coefficient of variation of each model's compartmental time constants $\tau_i = R_i C_i$, as a measure of how much physiologically distinct regional heterogeneity the model can represent Fig. 9

Under Scheme 1, the three-compartment model scored highest (68.0 vs. 64.7 and 56.0), remained top-ranked in 8 of 10 one-at-a-time weight perturbations (± 10 percentage points), and won 60.7% of 20,000 Monte Carlo trials sampled around the original weights (41.8% under fully uniform random weights). Under Scheme 2, the two-compartment model scored highest instead (58.9 vs. 55.0 and 45.0) and remained top-ranked in 7 of 10 one-at-a-time perturbations. However, this advantage did not carry through cleanly to the Monte Carlo analysis: when weights were sampled around the original scheme, the two- and three-compartment models won an almost equal share of trials (39.1% and 39.8%, respectively), both well ahead of the single-compartment model (21.1%); and under fully uniform random weights, the single-compartment model became the clear frontrunner (55.8%), well ahead of the two-compartment model (27.0%) and the three-compartment model (17.2%).

Neither scoring scheme can currently be considered more authoritative than the other without further clinical validation, and even within Scheme 2 the model favored at the single original weighting (two-compartment) is not the model favored once weight uncertainty is introduced (where two- and three-compartment are essentially tied, and single-compartment dominates under fully agnostic weights). The robust conclusions are therefore: (i) the model ranking is materially sensitive to how clinical applicability, parameter estimation ease, and model stability are operationalized, a sensitivity at least as large as that to the criterion weights themselves; and (ii) no single compartment count is an unconditionally optimal choice across all reasonable scoring and weighting assumptions tested here. This is treated as a general limitation of weighted decision-matrix approaches in this domain, and practitioners applying this matrix are advised to define and justify their own scoring of the qualitative criteria, and to test the resulting ranking's sensitivity to their specific weighting choices, before adopting a single top-ranked recommendation for their context.

5 Conclusion

This study successfully developed and evaluated electrical analog models for single, two, three, and multi-compartment respiratory systems to simulate human lung mechanics. The results demonstrate that while the single-compartment model is computationally efficient, it fails to capture the regional heterogeneity and uneven ventilation characteristic of diseased lungs. In contrast, the multi-compartment ($N = 10$) model, used throughout this study as a high-fidelity analytical reference rather than as a source of clinical validation, captures the full regional heterogeneity of the underlying lung by construction, and its computational cost (Table 6) makes it best suited to offline analysis rather than real-time bedside deployment. Among the three real-time candidate models, a weighted decision matrix and its accompanying sensitivity analysis (Sections IV-I–IV-J) showed that the top-ranked model depends on how the matrix's qualitative criteria are scored: an illustrative expert-judgment scoring favored the three-compartment model, while a fully formula-derived scoring favored the two-compartment model, and the single-compartment model became competitive with both once weight uncertainty was introduced. The two- and three-compartment models are therefore presented as the strongest candidates for intelligent ventilator monitoring and patient-specific respiratory control, with the choice between them depending on whether a given deployment prioritizes the clinical interpretability of a three-region split or the simplicity and numerical robustness of a two-region split, rather than a single configuration being unconditionally optimal.

Despite the internally consistent behaviour of the developed models, several limitations were identified during the study: Computational Latency: The execution time for the multi-compartment model (18.7 ms) exceeded the standard ICU ventilator sampling rate of 5–10 ms, limiting its current use for real-time bedside control. Model Simplification: In the simplified single-compartment model, airway inertance was neglected to reduce the governing equations to a first-order system, which may impact accuracy during high-frequency ventilation. Lumped Parameter Approach: The use of lumped electrical analogs assumes a simplified representation of respiratory variables, which may not fully capture the intricate 3D spatial dynamics of gas exchange in the alveoli. Absence of Patient Data: No patient or clinical ventilator data were used anywhere in this study. The "predictive accuracy" results reported in Section IV-G (Table 5) compare the reduced-order models against a high-fidelity $N = 10$ analytical reference model rather than against real physiological measurements; they should therefore be interpreted as a measure of internal model-order approximation quality, not as evidence of clinical validity. Validation against real patient or ventilator waveform data remains an essential step before any clinical application of these models. Decision-Matrix Sensitivity: As detailed in Section IV-J, the ranking of candidate models is materially sensitive to how qualitative decision criteria are scored and to the assumed criterion weights; this sensitivity should be re-examined by any practitioner applying this framework in a specific clinical context. Disease-Specific Parameterization: The present quantitative comparison used a single generically heterogeneous reference lung rather than distinct asthma-, COPD-, or ARDS-specific parameter sets; simulating and comparing models under explicit disease-specific parameterizations, with literature-sourced resistance and compliance ranges for each condition, is left for future work. Intratidal Mechanics: A further limitation is that the lumped-parameter models developed here assume time-invariant resistance and compliance values within a single breath. This does not reflect the intratidal (within-breath) changes in respiratory mechanics – such as progressive alveolar recruitment during inspiration and derecruitment during expiration – that are a clinically relevant feature of the injured lung, for example in ARDS. Viscoelastic or recruitment-dependent formulations, such as that proposed by Ganzert et al. [23], would be required to capture this behaviour and represent an important direction for extending the present models. Data Constraints: The simulation was conducted using parameters aggregated from an internally defined reference model rather than from direct, real-time patient trials. Parameter Estimation: The ease of parameter estimation decreases as model complexity increases, potentially complicating the rapid configuration of multi-compartment models in clinical settings.

Based on the findings of this research, the following recommendations are made for future developments: Real-Time Optimization: Future studies should focus on optimizing the numerical solution techniques for

multi-compartment models to bring their execution time within the 5–10 ms window required for real-time ventilator updates. Clinical Integration: The two- and three-compartment models should be evaluated for integration into smart respiratory support systems and patient-specific ventilator control algorithms, with the final selection informed by a context-specific weighting and scoring of the decision-matrix criteria in Section IV-J rather than by the single fixed weighting used here. Adaptive Control: It is recommended to implement these models within intelligent frameworks, such as fuzzy logic-based systems, to automate PEEP and FiO_2 adjustments based on the ARDS Berlin definition. Expanded Pathological Modeling: Future research should expand the models to include more specific parameters for a wider range of diseased conditions, such as pulmonary fibrosis and severe asthma, to improve diagnostic sensitivity. Clinical Validation: Prospective validation of these models against real patient or ICU ventilator waveform data, with appropriate ethical approval, is recommended as an essential next step before any of the findings in this study are interpreted as clinically validated.

Author contributions J.N.W simulated and M.R.A. wrote the manuscript.

Funding No funding was received.

Data availability The datasets used and/or analyzed during the current study are available from the corresponding author on reasonable request.

Code availability The Python code used to generate all simulated results, figures, and tables in this manuscript (Sections IV-F–IV-J) is publicly available under the MIT License at: https://github.com/wanzalajn/Code-to-Modeling-of-Human-Lung-Mechanics-Using-Multi-Compartment-Electrical-Circuit-Models.git

Declarations

Ethics approval and consent to participate Not applicable.

Consent for publication Not applicable.

Competing interests The authors declare no competing interests.

Open Access This article is licensed under a Creative Commons Attribution 4.0 International License, which permits use, sharing, adaptation, distribution and reproduction in any medium or format, as long as you give appropriate credit to the original author(s) and the source, provide a link to the Creative Commons licence, and indicate if changes were made. The images or other third party material in this article are included in the article's Creative Commons licence, unless indicated otherwise in a credit line to the material. If material is not included in the article's Creative Commons licence and your intended use is not permitted by statutory regulation or exceeds the permitted use, you will need to obtain permission directly from the copyright holder. To view a copy of this licence, visit http://creativecommons.org/licenses/by/4.0/.

References

1. Otis AB, McKerrow CB, Bartlett RA, Mead J, McIlroy MB, Selver-Stone NJ, et al. Mechanical factors in distribution of pulmonary ventilation. J Appl Physiol. 1956;8(4):427–43. https://doi.org/10.1152/jappl.1956.8.4.427.
2. Mead J. Mechanical properties of lungs. Physiol Rev. 1961;41(2):281–330. https://doi.org/10.1152/physrev.1961.41.2.281.
3. Palazzi E, Rovatti M, del Borghi M, et al. N-compartment mathematical model for the uptake and distribution of inhaled inert gases in the human body: an analytical solution. Med Biol Eng Comput. 1983;21:128–33. https://doi.org/10.1007/BF02441526.
4. Amilo D, Sadri K, Suleiman I, et al. A study on fractional-order lung cancer model under different internal influences with time delays analysis and modeling. Netw Model Anal Health Inform Bioinform. 2025;14:66. https://doi.org/10.1007/s13721-025-00567-5.
5. Said M, Roh Y, Jung IH. Mathematical modeling and analysis of leptospirosis-COVID-19 co-infection with real data. Eur Phys J Plus. 2024;139:1030. https://doi.org/10.1140/epjp/s13360-024-05846-0.

6. Dedam JPH, Fogel M, Fogel E. Respiratory system. In Diseases of the endocannabinoid system. Springer; 2025. https://doi.org/10.1007/978-3-031-87484-0_6.
7. Burtscher M, Philippe M, Vonbank K. Development of the respiratory system during adolescence. In Xu M, Xiao J, editors. Enhancing adolescent health (Advances in Experimental Medicine and Biology, Vol. 1505). Springer; 2026. https://doi.org/10.1007/978-981-95-7000-3_4.
8. Bush A. COPD: a pediatric disease. COPD: J Chron Obstruct Pulmon Dis. 2008;5(1):53–67.
9. Mendes R, Martins G, Battaglini D, Robba C, Silva P L, Rocco PRM. Brain–lung crosstalk and mechanical ventilation. In Battaglini D, De Rosa S, Godoy DA, editors. Organ system crosstalk in critical illness. Springer; 2025. https://doi.org/10.1007/978-3-032-01024-7_26.
10. Tomaz BS, Morais PAF, Holanda MA. Principles of mechanical ventilation. In Baptistella AR, Borges DL, Reis LFdF, editors. Weaning from mechanical ventilation. Springer; 2025. https://doi.org/10.1007/978-3-032-01145-9_1.
11. Bursa F, Frelich M, Sklienka P, et al. Protective mechanical ventilation controlled by real-time mechanical power measurement. J Clin Monit Comput. 2026;40:103–11. https://doi.org/10.1007/s10877-025-01369-w.
12. Suki B, Bates JHT. Lumped-parameter models of lung function. In Mathematical modeling of the healthy and diseased lung: Springer; 2025. https://doi.org/10.1007/978-3-031-95322-4_3.
13. Wanzala JN, Atim MR, Obungoloch J. Design of fuzzy logic-based ARDS Berlin definition for ventilator adjustments to ensure lung protection. Int J Fuzzy Syst. 2023;25:1935–51. https://doi.org/10.1007/s40815-023-01489-y.
14. Wanzala JN, Atim MR, Obungoloch J. Design of fuzzy logic-based ARDS berlin definition for ventilator adjustments to ensure lung protection. Int J Fuzzy Syst. 2023;25:1935–51. https://doi.org/10.1007/s40815-023-01489-y.
15. Wanzala JN, Atim MR, Obungoloch J. Design and simulation of a physician-based fuzzy system for ventilator adjustments in ARDS patients to ensure lung protection. Adv Fuzzy Syst. 2023;2023:3252763. https://doi.org/10.1155/2023/3252763.
16. Kuzminskas H, Teixeira MCM, Galvao RKH, et al. Tracking control of airflow based on a fractional-order model of lung impedance. Sci Rep. 2025;15:34832. https://doi.org/10.1038/s41598-024-77654-6.
17. Roy M, Bhattacharjee S, Neogi B, et al. Design and development of an implantable circuit for adjusting required pressure inside the respiratory system. Microsyst Technol. 2025;31:367–80. https://doi.org/10.1007/s00542-024-05694-z.
18. Chowdhury A, Baumert M. Respiratory mechanics: modelling, measurement, and clinical applications–a review. Biomed Eng Online. 2026;25:47. https://doi.org/10.1186/s12938-026-01537-2.
19. Mori K, Shirai T, Mikamo M, Shishido Y, Akita T, Morita S, et al. Colored three-dimensional analyses of respiratory resistance and reactance in COPD and asthma. COPD: J Chron Obstruct Pulmon Dis. 2011;8:456–63.
20. Park H, Lee HJ, Lee HW. Diagnosis and evaluation of small airway disease and COPD using impulse oscillometry. Sci Rep. 2024;14:28030.
21. Qawi I, Waybill K M. ARDS and respiratory failure. In Lanspa MJ, Levinson AT, editors. Echocardiography and ultrasonography in the ICU. Humana. 2025. https://doi.org/10.1007/978-3-031-80038-2_57.
22. Valda Toro PL, Willmore A, Wu NE, et al. Rapidly improving ARDS differs clinically and biologically from persistent ARDS. Crit Care. 2024;28:132. https://doi.org/10.1186/s13054-024-04883-6.
23. Ganzert S, Möller K, Steinmann D, Schumann S, Guttmann J. Pressure-dependent stress relaxation in acute respiratory distress syndrome and healthy lungs: an investigation based on a viscoelastic model. Crit Care. 2009;13:R199. https://doi.org/10.1186/cc8203.
24. Kretschmer J, Wahl A, Möller K. Dynamically generated models for medical decision support systems. Comput Biol Med. 2011;41(10):899–907.

Publisher's Note Springer Nature remains neutral with regard to jurisdictional claims in published maps and institutional affiliations.

Authors and Affiliations

Jimmy Nabende Wanzala[1] · Michael Robson Atim[2]

✉ Jimmy Nabende Wanzala
wanzalajimmy@gmail.com

Michael Robson Atim
mikeatim.sci@busitema.ac.ug

[1] Physics department, Mbarara University of Science and Technology, Mbarara, Uganda

[2] Physics department, Mbarara University of Science and Technology, Tororo, Uganda